

PACS numbers: 81.05.Je; 81.05.Mh; 42.62.Cf
DOI: 10.1070/QE2009v039n02ABEH013749

Physical mechanisms of CO_2-laser-induced rapid structural changes in glass-ceramics

V.P. Veiko, E.B. Yakovlev, E.A. Shakhno

***Abstract*. Laser-induced local structural changes in glass-ceramics have recently been the subject of intense research interest in connection with analytical, aerospace, optical-memory and other advanced applications. In this paper, we demonstrate that important features of such processes are very high rates and unusual kinetics. These features are interpreted in terms of thermophysical kinetics and a novel view of amorphous materials as vacancy-distorted crystals.**

Keywords: *glass-ceramics, laser processing, crystallisation, amorphisation, thermophysical kinetics.*

1. Introduction

As a class of materials, glass-ceramics (GCs) have been known since the 1950s, which saw the advent of polycerams in the United Kingdom and sitalls in the USSR [1]. Basically, GCs are polycrystalline materials prepared from glass containing crystal-forming substances (nucleating agents) by heat treatment for 6 – 10 h. The crystallisation process begins with the formation of billions of submicroscopic nuclei per cubic millimetre, each serving as a growth centre. Owing to the great diversity of glass compositions and heat-treatment procedures, GCs offer a variety of properties [1].

In contrast to conventional glass, whose properties are determined primarily by its chemical composition, in the case of GCs a key role is played by their microcrystalline structure and phase composition. In addition to being similar in manufacturing process, various GCs contain silica as a key component and consist of both glassy and crystalline phases.

Thus, GCs constitute a class of polycrystalline materials prepared by directional (catalysed) crystallisation of glasses with special compositions. GCs contain one or several crystalline phases uniformly distributed over an amorphous phase. Characteristically, GCs combine high hardness and mechanical strength with excellent insulating properties, high softening temperature, thermal and chemical stability and other features, due to their fine-grained, uniform semicrystalline structure. Local amorphisation of GCs, resulting in optical transparency and influencing their surface morphology by virtue of the amorphisation-induced increase in specific volume, makes them candidate materials for micro- and nanophotonic applications [2] (Fig. 1). Owing to the large difference in solubility and ion-exchange properties between their amorphous and crystalline components, GCs can be used equally successfully to produce both surface and bulk structures for lab-on-a-chip devices [3, 4], so-called nanosatellites [4, 5], diffraction gratings [6] and other applications.

As mentioned above, glass crystallisation in the GC fabrication process involves several prolonged heating/cooling steps [1]. At the same time, our experiments [3] have shown that, under CO_2 laser irradiation, the structural and phase changes involved occur very rapidly, taking in the order of several seconds. The mechanisms of these rapid structural changes are not yet fully clear. A detailed understanding of these mechanisms would allow one to create advanced optical materials with tailored properties and to substantially extend the application area of GCs.

The objective of this work was to review the recent developments in experimental studies of laser amorphisation and crystallisation in GCs and, more importantly, to analyse and interpret the results obtained.

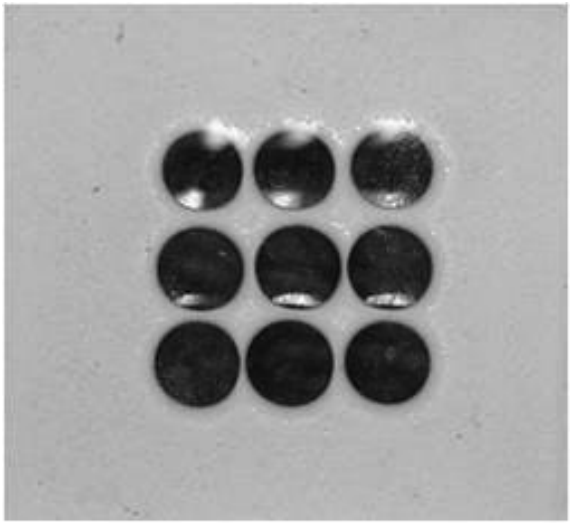

Figure 1. Reflected-light photograph of a plate with an array of high-quality microlenses produced by laser amorphisation of Sitall ST-50 (lens diameter, 0.9 mm; total fabrication time, $\sim$ 1 min).

V.P. Veiko, E.B. Yakovlev, E.A. Shakhno St. Petersburg State University of Information Technologies, Mechanics and Optics, Kronverkskii prosp. 49, 197101 St. Petersburg, Russia; e-mail: veiko@lastech.ifmo.ru

Received 1 November 2007; revision received 10 July 2008
Kvantovaya Elektronika **39** (2) 185 – 190 (2009)
Translated by O.M. Tsarev

The key features of structural modification to GCs will be illustrated by the amorphisation of Sitall ST-50-1, which consists mainly of rutile (α-TiO_2), cordierite ($2MgO \times 2Al_2O_3 \cdot 5SiO_2$) and an amorphous phase (SiO_2, 60.5; Al_2O_3, 13.5; CaO, 8.5; MgO, 7.5; TiO_2, 10 wt %), and also by the crystallisation of the titanium-containing glass obtained through laser-heating-induced amorphisation of ST-50-1. Note that ST-50-1 strongly scatters visible light and is thus opaque in the visible to near-IR spectral region even at thicknesses just under 1 mm.

2. Experimental results

Our experimental results have been presented in recent publications, so here we only outline them. For more details, we refer the reader to previous reports [7, 8].

Our experimental setup is shown schematically in Fig. 2. It comprises a laser processing system and two measurement systems, one for measuring the temperature T of the zone being heated, heating rate (v_{heat}) and cooling rate (v_{cool}), and the other for measuring the visible transmittance of the GCs during CO_2 laser irradiation.

The transmission measurements are intended to assess the bleaching or darkening rate as the amorphisation or crystallisation front advances deeper into the sample. Micro-video imaging is used to determine the radial growth rate of the bleached zone.

The phase composition and structural state of GCs were identified by standard X-ray diffraction (XRD) techniques. Figure 3a shows the XRD pattern of the unprocessed GCs. The peaks at 1.688 and 2.495 Å are due to rutile (α-TiO_2), the halo around 3.505 Å is characteristic of amorphous SiO_2, and the other peaks arise from cordierite ($2MgO \times 2Al_2O_3 \cdot 5SiO_2$). The relative area of the grey regions represents the amorphous content of the GCs. Bleaching occurs when crystals, which have strongly scattering boundaries, disappear (Fig. 3b), and the amorphous content rises. As a result of the amorphisation process, the transmission band of the material shifts from the mid-IR (with a maximum at $\lambda \sim 5.5$ μm) to the visible/near-IR region, 0.3–2.8 μm (Fig. 4), extending up to 5 μm. At incident power densities and heating rates below those needed for amorphisation, ST-50-1 crystallises, as evidenced by XRD results (Fig. 3c), optical spectra of recrystallised GCs (Fig. 4) and the visual appearance of unprocessed, amorphised and recrystallised GCs. Figure 5 shows typical time dependences

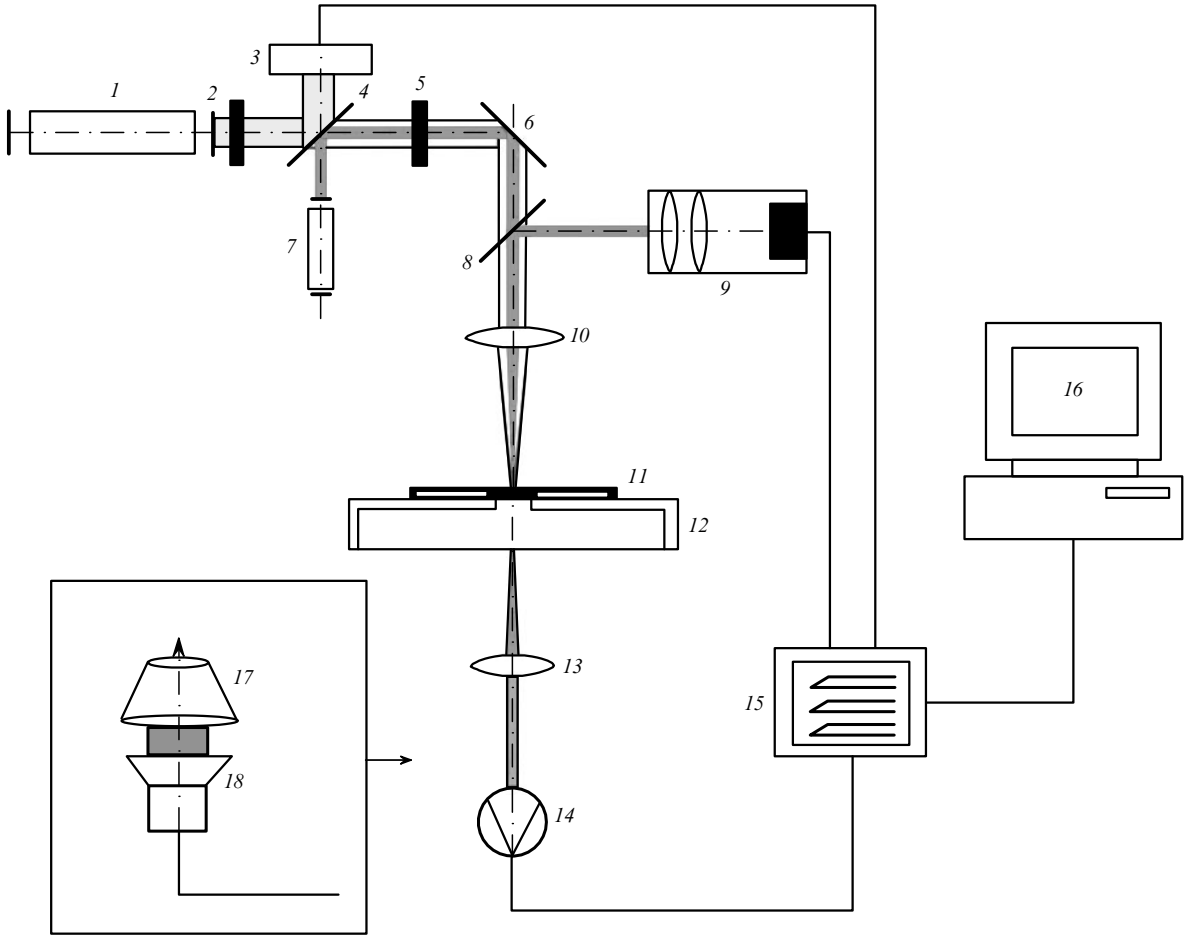

Figure 2. Scheme of the experimental setup.
High-power laser processing system: (*1*) CO_2 laser; (*2*) gate; (*3*) power meter; (*5*) aperture; (*6, 8*) mirrors; (*10*) ZnSe lens; (*11*) GC sample; (*12*) *x*–*y* stage.
Temperature measurement system: (*9*) digital pyrometer; (*15*) multichannel interface; (*16*) computer.
Transmission measurement system: (*4*) beamsplitter; (*7*) He–Ne laser; (*10, 13*) lenses; (*14*) photodetector; (*15*) multichannel interface; (*16*) computer; (*17*) microscope; (*18*) video camera.

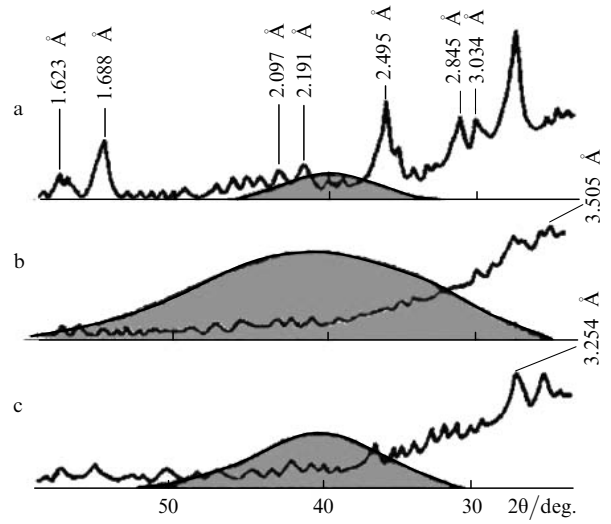

Figure 3. XRD patterns of (a) unprocessed, (b) amorphised (after exposure to laser light) and (c) partially recrystallised (after a second exposure) GCs.

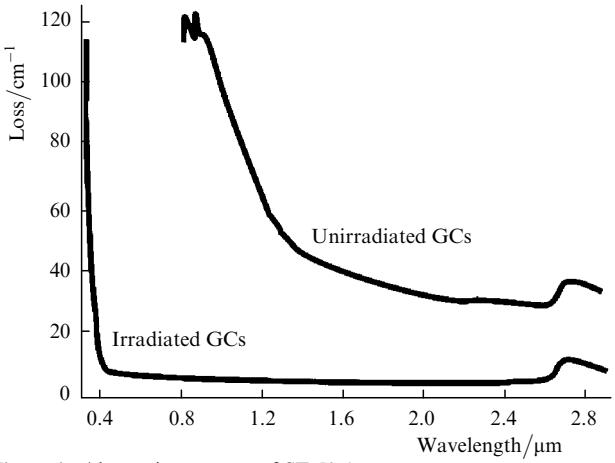

Figure 4. Absorption spectra of ST-50-1.

of the surface temperature over one heating/cooling cycle for a 0.6-mm-thick sample under CO_2 laser irradiation at a laser spot diameter of 1 – 2 mm and various incident power densities.

Laser amorphisation occurs at heating rates $v_{heat} \sim 30 - 80$ K s^{-1} and cooling rates $v_{cool} \sim 50 - 100$ K s^{-1}. In this process, the temperature of the zone being heated reaches the melting point T_{melt}, and the rate of subsequent cooling is high enough for melt freezing and the formation of a stable, fracture-free amorphous material.

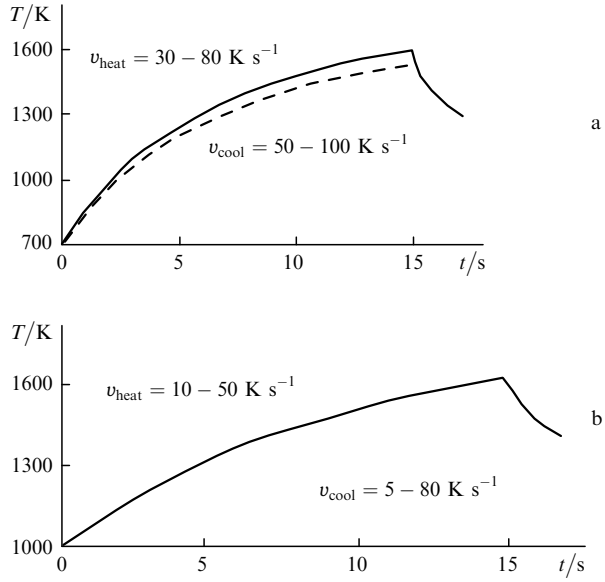

Figure 5. Surface temperature of ST-50-1 under laser irradiation: (a) amorphisation (incident power $P = 1 - 3$ W, power density $q = 3 \times 10^5$ to 3×10^6 W m^{-2}, initial temperature $T_0 = 700$ K); (b) crystallisation ($P \leqslant 0.3$ W, $q \leqslant 10^5$ W m^{-2}, $T_0 = 1000$ K).

After laser irradiation, the molten zone continues to grow for some time and then begins to decrease, whereas the dimensions of the amorphised zone stabilise. Increasing the dimensions of the amorphised zone reduces the cooling rate, which is conducive to glass crystallisation at the periphery of the amorphised zone.

The formation of amorphised and recrystallised zones in GCs during laser irradiation is illustrated in Fig. 6.

Figure 7 plots the dimensions of the amorphised zone versus time (data obtained by optical microscopy of cross-sectional samples and micro-video imaging).

Figure 8 illustrates the effect of the CO_2 laser output power on the melting-through time in the centre of the zone under irradiation, the complete amorphisation time and the complete crystallisation time.

3. Discussion

3.1 GC amorphisation process

We associate this process with laser melting of GCs followed by amorphisation as a result of rapid cooling. Note first of all that we do not assume that rutile and cordierite microcrystals, typically present in ST-50-1, undergo complete melting. Their presence in the amorphous

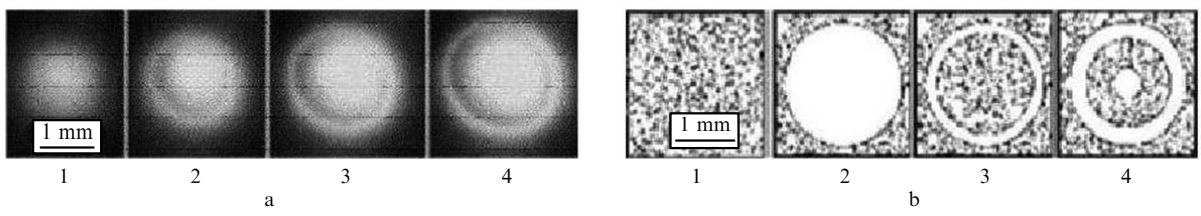

Figure 6. (a) Formation of an amorphised GC zone under laser irradiation; (b) photographs of the sample after a second exposure at different beam diameters; the unprocessed and recrystallised zones appear grey, and the amorphised zone appears white; the images were taken after exposure for (1) 6, (2) 6.5, (3) 7 and (4) 8 s.

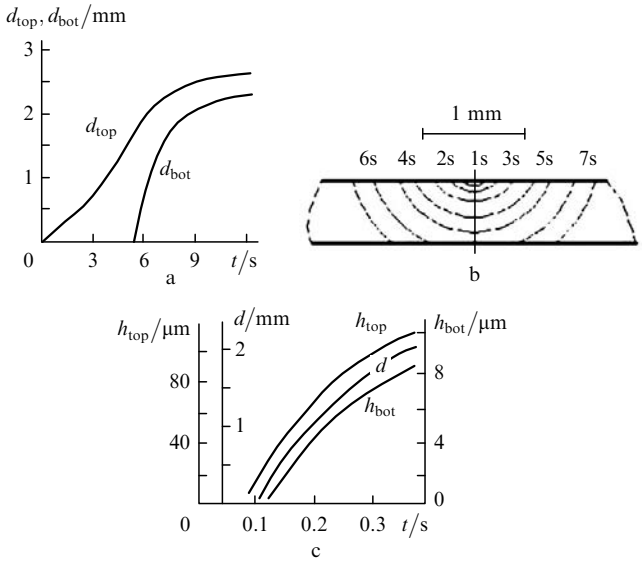

Figure 7. Amorphisation kinetics: (a) increase in the top (d_{top}) and bottom (d_{bottom}) diameters of the amorphised zone, (b) amorphisation front advancement and (c) increase in the depth and diameter of the amorphised zone ($d_0 = 1$ mm, $h = 0.6$ mm, $q = 5 \times 10^6$ W m^{-2}, $T_0 = 800$ K).

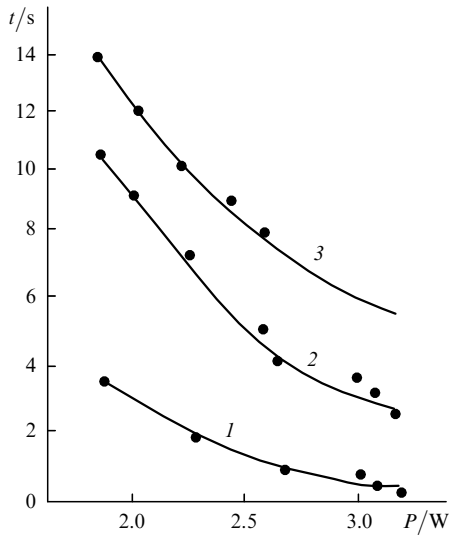

Figure 8. (*1*) Melting-through time in the centre of the zone under irradiation, (*2*) complete amorphisation time and (*3*) complete crystallisation time as functions of CO_2 laser output power ($T_0 = 935$ K, $h = 0.6$ mm, $r_0 = 0.7$ mm).

matrix is evidenced by characteristic XRD peaks (Figs 3b, 3c). It is these microcrystals which we believe to be responsible for the residual absorption in the GCs (~ 20 %).

Bleaching kinetics are governed by the rate at which the melting front advances into the bulk of the material. Rigorous thermophysical calculations of the melting/amorphisation process in question present serious problems because the temperature field of a GC plate being heated by laser radiation has a complex three-dimensional (3D) configuration and is nonstationary. Here, we restrict ourselves to estimating the heating rate at the beginning of surface melting and during the radial expansion of the molten zone.

In the initial stage of the process, laser exposure leads to heating of the region adjacent to the zone under irradiation. The heating rate at the beginning of melting, when the surface temperature T_{surf} reaches the melting point T_{melt}, can be determined by solving a 1D problem of heating of a strongly absorbing semi-infinite body [9]. The temperature in the centre of the laser spot is given by

$$T = \frac{2q(1-R)\sqrt{at}}{\sqrt{\pi}k} + T_0, \tag{1}$$

where R is surface reflectance, k and a are the thermal conductivity and thermal diffusivity of the material, t is the exposure time, and q is the incident laser power density.

The surface heating rate is

$$v_{heat} = \left.\frac{dT_{surf}}{dt}\right|_{T_{surf}=T_{melt}} = \frac{2q^2a(1-R)^2}{\pi k^2(T_{melt}-T_0)}. \tag{2}$$

At $q = 10^6$ W m^{-2} and $T_0 = 800$ K, v_{heat} is 3×10^3 K s^{-1}. Subsequently, as the rate of heat removal from the zone under irradiation increases, the heating rate drops, and the heat flow pattern in the plate becomes substantially 3D. The through-thickness average temperature in the centre of the area being irradiated is [10]

$$T_{av} = \frac{q(1-R)t}{\rho ch}\left[1 - \exp\left(-\frac{r_0^2}{4at}\right) - \frac{r_0^2}{4at}E_1\left(\frac{r_0^2}{4at}\right)\right] + T_0, \tag{3}$$

where ρ and c are the density and heat capacity of the material, and $E_1(z)$ is the exponential integral of order one.

Equation (3) can be used to determine the time derivative of the through-thickness average temperature in the centre of the laser spot, dT_{av}/dt, at an arbitrary instant in time. At an incident power density $q = 10^6$ W m^{-2} and spot radius $r_0 = 1$ mm, dT_{av}/dt varies from 40 K s^{-1} at $t = 1$ s to 5 K s^{-1} at $t = 10$ s. Under the above assumptions, the bleaching time t_{bleach} can be estimated as the time needed for uniformly heating a cylinder of diameter d_0 and height h from the preheating temperature T_0 to the melting point T_{melt}:

$$t_{bleach} = \frac{\rho ch(T_{melt}-T_0)}{q(1-R)}.$$

At $T_{melt} - T_0 = 250$ K and $q = 0.5 \times 10^6$ W m^{-2}, the bleaching time is 1.3 s. Taking into account lateral heat removal and the increase in the diameter of the molten zone by $\sqrt{a\tau}$ ($d_{melt} = d_0 + 2\sqrt{a\tau}$, where τ is the irradiation time) t_{bleach} increases to 2.7 s. These estimates agree well with experimental data (Fig. 5a), thus leaving no doubt that the amorphisation process is of a thermal nature.

Whether the solidified melt is amorphous or crystalline depends on the cooling rate and the nature of the melt. It can be shown theoretically that any melt can be amorphised by sufficiently fast cooling. To this end, consider the equation for the volume of the crystalline phase formed over time t_{cool} during glass cooling from the liquidus temperature to the glass transition temperature T_g. At a small volume of the crystalline phase, V, the equation has the form [11]:

$$V \approx V_0 \int_0^t I(t')V_t(t',t)\mathrm{d}t' \quad (V/V_0 \ll 1), \tag{4}$$

Here, V_0 is the initial melt or glass volume; $I(t')$ is the volume nucleation rate at time t'; $V_t(t',t) = \frac{4\pi}{3}[\int_{t'}^{t} c(t',t'')\mathrm{d}t'']^3$ is the volume at time t of a crystal that nucleated at time t', where $c(t',t'')$ is the linear growth rate of crystals, which are taken to be spherical in shape, of radius $R(t',t) = \int_{t'}^{t} c(t',t'')\mathrm{d}t''$.

Let ΔT be the temperature range in which the Ic^3 product has the highest value, and let the cooling rate of the melt, v_{cool}, be constant. Then the time needed for cooling by ΔT is $\Delta T/v_{\mathrm{cool}}$ and, from (4), we obtain a rough glass-forming criterion:

$$\frac{V}{V_0} \approx \overline{Ic^3}\left(\frac{\Delta T}{v_{\mathrm{cool}}}\right)^4 \ll 1, \tag{5}$$

where $\overline{Ic^3}$ is the average of Ic^3 over the temperature range ΔT. In practice, the solidified melt can be considered amorphous at $V/V_0 \approx 10^{-6}$.

Thus, since GC amorphisation requires melting followed by rapid melt cooling (to avoid recrystallisation), we think that the key process parameters are the temperature of the GCs, the heating and cooling rates and the bleaching front advancement rate, which were determined in our experiments.

3.2 Crystallisation process

As mentioned above, the melt obtained by laser exposure is considered to be in a nonequilibrium state, with residual traits of the parent crystalline phase. The short-range order of ST-50-1 and probably the structure of the main types of crystals in the parent material continue to manifest themselves after melting and amorphisation; in particular, the crystallite size decreases, as evidenced by small-angle X-ray scattering data (Fig. 3b) and the residual absorption in the amorphised material (Fig. 4).

The above allows our experimental data to be interpreted in terms of vacancy-mediated melting, a model formulated by J. Frenkel and further developed by Yakovlev [12]. According to this model, the loss of long-range order on melting of polycrystals is the result of vacancy-induced lattice distortions. Supercooled melts retain high concentrations of vacancies, which are responsible for viscous flow of the melt. This may lead to fluctuation-assisted formation of crystalline nuclei, which contain lower vacancy concentrations, at the level of crystalline material.

In this situation, density and structure fluctuations may be of importance. In the case of local laser heating, such fluctuations are inherently due to the extremely sharp temperature gradient. The temperature gradient is a fundamental characteristic of laser irradiation, associated with rapid heating and cooling. It always gives rise to density fluctuations in the same direction and can be estimated as $\partial T/\partial x \approx \sqrt{\tau/a}\,\partial T/\partial t \sim 10^4$ K cm^{-1} at $\partial T/\partial t \sim 100$ K s^{-1}.

In more rigorous terms, the surface temperature gradient is determined by two main factors: the intensity distribution over the laser spot and the radial heat flux. From an analysis of the thermal field, the temperature gradient near the melting isotherm can be estimated as

$$\mathrm{grad}T \approx \xi \frac{T_{\mathrm{surf}} - T_0}{r_0 + 4a\tau/r_0}, \tag{6}$$

where $\xi = 2-5$, depending on processing conditions. Therefore, the temperature gradient near the melting isotherm is $100-300$ K cm^{-1}.

Indirect evidence for the important role of the temperature gradient is provided by Fig. 9, which illustrates GC crystallisation during CO_2 laser irradiation. The photograph shows clearly that crystallisation occurs along the temperature gradient. Under certain conditions, the crystallised zones grow as a consequence of vacancy outdiffusion and recombination at the boundary of the amorphous phase. Since the diffusion rate in silicate glass is rather slow, the growth of a crystalline phase through concentration-driven diffusion requires considerable time (hours).

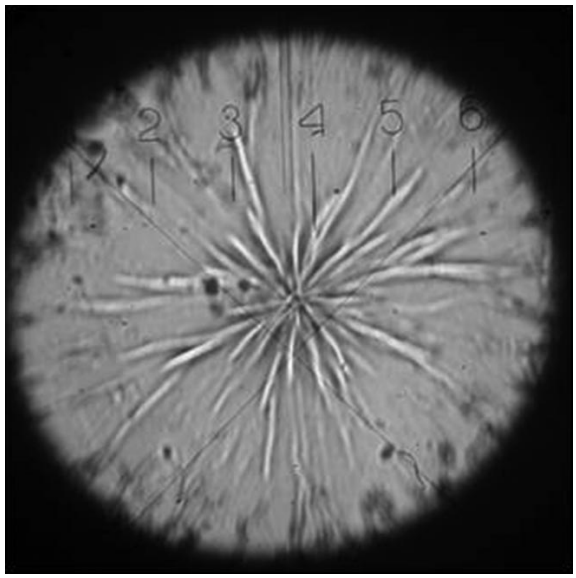

Figure 9. Photograph illustrating the initial stage of crystallisation in the irradiated zone.

After rapid (within seconds) heating of glass to its crystallisation temperature, the vacancy concentration is below the equilibrium value. Under such conditions, the vacancy distribution over the material is nonuniform, and there are regions more similar in properties to crystals (below-average vacancy concentration) or to the equilibrium melt (above-average vacancy concentration).

The reduction in vacancy concentration in 'crystallizing' regions is then due not to vacancy recombination but to vacancy flow from a region with a low concentration to one with a higher concentration. In the absence of slow vacancy diffusion processes, laser crystallisation occurs more rapidly because it is no longer diffusion-limited.

Let us estimate laser irradiation parameters at which rapid crystallisation is possible.

The rate of vacancy generation during heating can be estimated as [12]

$$v_{\mathrm{vac}} \sim \frac{N^{2/3}}{\tau} S_{\mathrm{flow}} \exp[-E_{\mathrm{vac}}/(k_{\mathrm{B}}T)], \tag{7}$$

where N is the oxygen concentration; $\tau \sim 10^{-13}$ s, S_{flow} is the vacancy sink area (boundary area); E_{vac} is the vacancy formation energy, and k_{B} is the Boltzmann constant.

The number of vacancies formed during heating for time t is then given by

$$N_{\rm vac} \sim \frac{N^{2/3}}{\tau\delta} S_{\rm flow} \int_0^t \exp[-(E_{\rm vac}+E_{\rm d})/(k_{\rm B}T)]{\rm d}t$$

$$= \frac{N^{2/3}}{\tau\delta} S_{\rm flow} \int_0^t \frac{\exp[-(E_{\rm vac}+E_{\rm d})/(k_{\rm B}T)]}{{\rm d}T/{\rm d}t}{\rm d}T, \qquad (8)$$

where $E_{\rm d}$ is the activation energy for vacancy diffusion and δ is the lattice constant of the crystal.

Since vacancies are formed mostly at high temperatures, the integral in (8) can be estimated as

$$N_{\rm vac} \sim \frac{N^{2/3}}{\tau\delta} S_{\rm flow} \frac{\exp[-(E_{\rm vac}+E_{\rm d})/(k_{\rm B}T)]k_{\rm B}T^2}{(E_{\rm vac}+E_{\rm d}){\rm d}T/{\rm d}t}. \qquad (9)$$

For the above process to take place, $N_{\rm vac}$ must be below the equilibrium vacancy concentration in a supercooled melt, $N_{\rm vac} < N_{\rm vac\,0}$. Given that $N_{\rm vac\,0} = N\exp[-E_{\rm vac} \times (k_{\rm B}T)^{-1}]$, we obtain from (9) for $N_{\rm vac} < N_{\rm vac\,0}$

$$\frac{{\rm d}T}{{\rm d}t} > \frac{k_{\rm B}T^2}{\tau(E_{\rm vac}+E_{\rm d})} \exp\left(-\frac{E_{\rm d}}{k_{\rm B}T}\right). \qquad (10)$$

At 500 K $\tau \sim 10^{-13}$ s, $E_{\rm d}/(k_{\rm B}T) \approx 37$ и $S_{\rm flow} = 1$ cm^2 (estimates per unit volume), we obtain ${\rm d}T/{\rm d}t \approx 50$ K s^{-1}, in agreement with experimental data.

In the case under consideration, the structure of crystals resembles that of the supercooled melt where crystallisation occurs. Moreover, with this crystallisation mechanism the melt never crystallises completely because vacancy diffusion to the bulk of the glass is needed, as observed in our experiments.

4. Conclusions

Our experimental results and theoretical analysis lead us to the following conclusions:

1. Laser amorphisation of polycrystalline GCs and the kinetics of this process can be fully understood in terms of the proposed thermophysical model (heating, melting, cooling) for the interaction of laser radiation with materials in an equilibrium state.

2. Rapid laser crystallisation of amorphous (glassy) materials can only be explained by taking into account the key features of their behaviour in a nonequilibrium state. To adequately account for this process, it is necessary to assume that the melt resulting from rapid laser heating contains residual quasi-ordered polycrystalline structures, which play a key role in the crystallisation process. Our data provide evidence of such structures.

Acknowledgements. This work was supported by the Russian Foundation for Basic Research (Grant Nos 07-02-00887-a and 07-02-00894-a), the Federal Agency for Education (State Contract No. RNP 2.1.1.784) and in part by NATO (Project No. CBP.EAP.CLG 982748). The authors are grateful to B.Yu. Novikov for his assistance in preparing the manuscript.

References

1. Berezhnoi A.I. *Glass-Ceramics and Photo-sitalls* (New York: Plenum, 1970; Moscow: Mashinostroenie, 1966).
2. Sugioka K., Cheng Y., Masuda M., Midorikawa K., Shihoyama K. *Proc. SPIE Int. Soc. Opt. Eng.*, **5399**, 1 (2003).
3. Veiko V.P., Kieu Q.K. *Kvantovaya Elektron.*, **37**, 92 (2007) [*Quantum Electron.*, **37**, 92 (2007)].
4. Cheng Y., Sugioka K., Midorikawa K. *Proc. SPIE Int. Soc. Opt. Eng.*, **5662**, 209 (2004).
5. Fuqua P., Janson S.W., Hansen W.W., Helvajian H. *Proc. SPIE Int. Soc. Opt. Eng.*, **3618**, 213 (1999).
6. Skiba P.A. *Lazernaya modifikatsiya steklovidnykh materialov* (Laser Modification to Glassy Materials) (Minsk: BGU, 1999) p. 132.
7. Veiko V.P., Kieu Q.K., Nikonorov N.V., Skiba P.A. *J. Laser Micro/Nanoengineering*, **1** (2), 149 (2006).
8. Veiko V.P., Kromin A.K., Yakovlev E.B. *Proc. SPIE Int. Soc. Opt. Eng.*, **1992**, 159 (1993).
9. Metev S.M., Veiko V.P. *Laser-Assisted Microtechnology* (New York, Heidelberg: Springer Verlag, 1998).
10. Veiko V.P., Libenson M.N. *Lazernaya obrabotka materialov* (Laser Processing of Materials) (Leningrad: Mashinostroenie, 1973).
11. Filipovich V.N., Kalinina A.M., Sychova G.A., in S*tekloobraznoe sostoyanie* (Glassy State) (Leningrad: Nauka, 1988) pp 87–96.
12. Yakovlev E.B. *Opt. Zh.*, **63** (2), 5 (1996).